The 21th Cambridge Workshop on Cool Stars, Stellar Systems, and the Sun
Edited by A. S. Brun, J. Bouvier, P. Petit

Nonlinear tidal interactions in the convective envelopes of low-mass stars and giant gaseous planets

Aurélie Astoul,[1] Adrian Barker[1]

[1]Department of Applied Mathematics, School of Mathematics, University of Leeds, Leeds, LS2 9JT, UK

1 *

Abstract In close exoplanetary systems, tidal interactions are known to shape orbital architectures, to modify star and planet spins, and to have an impact on the internal structures of the bodies through tidal heating. Most stars around which planets have been discovered are low-mass stars and thus feature a convective envelope, as is also expected in giant gaseous planets like Hot Jupiters. Tidal flows in convective envelopes consist of large-scale equilibrium tides and inertial waves (restored by the Coriolis acceleration, and recently discovered in the Sun) excited by tides. Inertial waves contribute greatly to the tidal dissipation when they are excited and subsequently damped (through e.g. turbulent viscous friction), especially early in the life of a system. These waves are known to be subject to nonlinear effects, including triggering differential rotation in the form of zonal flows. In this context, we investigate how nonlinearities affect tidal properties, thanks to 3D nonlinear hydrodynamical simulations of tidal flows, in an adiabatic and incompressible convective shell. Unlike previous studies, we use a realistic tidal body forcing to excite inertial waves. Within our new set-up, we observe the establishment of strong cylindrically-sheared zonal flows, which modify the tidal dissipation rates from prior linear theoretical predictions. We demonstrate that the effects of this differential rotation on the waves neatly explains the discrepancies between linear and nonlinear dissipation rates in many of our simulations. Nonlinear interactions between inertial waves, and those between the waves and the background sheared flow, can lead to instabilities, for sufficiently high tidal forcing amplitudes or low viscosities. These different processes disrupt the energetic exchanges between tidal waves and the background flow, and also further modify tidal dissipation rates.

2 Introduction

Due to the compact nature of many exoplanetary systems discovered so far, the study of tidal interactions is essential to understand the orbital and rotational properties of the planets, as well as the rotations of their host stars. There has been a growing interest in detecting orbital decay of close Hot Jupiters, presumably caused by tidal interactions (e.g. Patra *et al.*, 2020; Harre *et al.*, 2023). Though many ∼one-day orbital period giant gaseous planets are expected to migrate towards their host stars if tides are strong, only WASP-12 b has been convincingly confirmed to decay to date (Maciejewski *et al.*, 2016). Therefore, an accurate theoretical estimation of tidal dissipation is needed to interpret the orbital decay rate of the planet/accelerating spin of star. In the WASP-12 system, non-linear wave breaking of gravity waves (restored by buoyancy) in the radiative central portions of the host star is believed to be responsible for the inward spiralling of the planet (Chernov *et al.*, 2017; Weinberg *et al.*, 2017; Barker, 2020). In other systems where this mechanism probably cannot apply, tidal dissipation of inertial waves (restored by the Coriolis acceleration) in stellar convective envelopes could be another avenue to explain any inferred orbital decay, as in the KELT-1 Hot Jupiter/brown dwarf system (Maciejewski *et al.*, 2022) or for the Hot Jupiter Kepler-1658 b (Vissapragada *et al.*, 2022). Given the high tidal forcing amplitudes[1] $\epsilon = (M_2/M_1)(R_1/a)^3$ expected in Hot Jupiters themselves, with a maximum $\epsilon \approx 6 \cdot 10^{-2}$ reached in WASP-12 b[2], nonlinear effects on tidally-excited inertial waves (particularly short-scale ones) are likely to be important in gaseous planets. For their host stars, $\epsilon \approx 4 \cdot 10^{-4}$ is perhaps the maximum value (for now), as reached in KELT-1, but it will be higher in the closest stellar binary systems. Among the few numerical studies dedicated to the impact of nonlinearities on tidally-excited inertial waves in a convective shell, (Favier *et al.*, 2014) have shown that tidal dissipation rates could be altered by several orders of magnitude compared with linear predictions, and are thus essential to study further. They also observed signs of sustained de-synchronisation of the primary body compared to the orbit, which is unexpected behaviour. In (Astoul & Barker, 2022), we built upon this work by using a more realistic treatment of tidal forcing in a 3D numerical model of a spherical shell modelling the convective envelope of either a low-mass star or a gaseous planet. The use of a wavelike/non-wavelike decomposition of the tidal flow allowed us to rule out the unexpected rotational evolution found by (Favier *et al.*, 2014). We were thus able to obtain new estimates of the tidal dissipation and to characterise nonlinear outcomes like zonal flows and instabilities. This conference proceedings article is intended as a short summary of the paper we published after the Cool Stars 21 conference (Secs. 3 and 4.1). In addition, we explore further some aspects, including simulations featuring corotation resonances (where the Doppler-shifted wave frequency vanishes locally) in order to understand better the presence or the absence of

[1]A measure of the strength of the tides with M the mass, R the radius and a the orbital semi-major axis, with subscripts 1 and 2 referring to the perturbed body and the perturber, respectively (Ogilvie, 2014)

[2]Using the exoplanet database `https://exoplanets.eu`.

instabilities (Sec. 4.2).

3 Tides in spherical shell model

Tides are studied in an incompressible, rotating, and adiabatic convective spherical shell, with stress-free and impenetrable boundary conditions. The tidal flow is decomposed as

$$\boldsymbol{u} = \boldsymbol{u}_{\rm nw} + \boldsymbol{u}_{\rm w}, \tag{1}$$

with subscripts referring to the non-wavelike (equilibrium) and wavelike (dynamical) components, respectively. The latter are tidally-forced inertial waves satisfying $|\omega| \leq 2\Omega$, with ω the tidal forcing frequency in the rotating frame of constant spin rate Ω. The former satisfies a set of time-dependent equations (the momentum, continuity, and Poisson equations along with the leading order quasi-hydrostatic equilibrium), but is assumed to be perfectly maintained on the timescale of our simulation, which is meant to be short in comparison with typical timescales of tidal evolution. By considering solely the quadrupolar tidal component when expanding in terms of spherical harmonics (Y_l^m of harmonic degree and order $l = m = 2$), which is the dominant one for asynchronous tides in a coplanar two-body system, the non-wavelike (equilibrium) flow can be shown to be:

$$\boldsymbol{u}_{\rm nw} = {\rm Re}\{-{\rm i}\omega C_{\rm T} \boldsymbol{\nabla}\left[f(r) Y_2^2(\theta,\varphi)\right] {\rm e}^{-{\rm i}\omega t}\}, \tag{2}$$

where $C_{\rm T} \approx \epsilon$ is the tidal forcing amplitude (higher for compact systems), and $f(r)$ is a radial function depending also on the radial aspect ratio α (the ratio of inner to outer radii; Ogilvie, 2013; Astoul & Barker, 2022). We have adopted units of length equal to the planetary/stellar radius (R) and time equal to Ω^{-1}. The system of equations for tidally-excited inertial waves in the fluid frame is:

$$\begin{gathered}\partial_t \boldsymbol{u}_{\rm w} + (\boldsymbol{u}_{\rm w}\cdot\boldsymbol{\nabla})\boldsymbol{u}_{\rm w} + 2\boldsymbol{\Omega}\wedge\boldsymbol{u}_{\rm w} = -\frac{\boldsymbol{\nabla} p_{\rm w}}{\rho} + \boldsymbol{f}_{\rm t} + \nu\Delta\boldsymbol{u}, \\ \boldsymbol{\nabla}\cdot\boldsymbol{u} = 0,\end{gathered} \tag{3}$$

with $p_{\rm w}$ the wavelike pressure and ρ the constant density. Here $\boldsymbol{f}_{\rm t} = -2\boldsymbol{\Omega}\wedge\boldsymbol{u}_{\rm nw}$ is the Coriolis acceleration on the non-wavelike flow, which acts as an effective tidal body force (see e.g. Ogilvie, 2005, 2013). The parameter ν is an effective viscosity modelling the action of convection on tides. Note that we have neglected the non-linear coupling between non-wavelike and wavelike flows here[3]. The volume averaged tidal dissipation in the shell is defined as $D_\nu = \langle\rho\nu\boldsymbol{u}_{\rm w}\cdot\boldsymbol{\Delta}\boldsymbol{u}_{\rm w}\rangle$.

4 Nonlinear effects on tidal dissipation

4.1 Tidally-induced geostrophic zonal flows

The system in Eq. (3) is solved by the magneto-hydrodynamical 3D pseudo-spectral code MagIC[4]. We fixed the Ekman number ${\rm E} = \nu/(\Omega R^2)$ to 10^{-5} (e.g. Bekki *et al.*, 2022) for an envelope as thick as the core ($\alpha = 0.5$), where R is the outer radius. The nonlinear self-interaction of inertial waves along their shear layers triggers cylindrical differential rotation in the form of quasi-geostrophic zonal flows. These are particularly powerful close to the reflection points at inner or outer boundaries or with the rotation axis, where the linear dissipation is expected to be important (Tilgner, 2007; Favier *et al.*, 2014; Astoul & Barker, 2022). The closer we are to a resonant peak of linear tidal dissipation (linked to the strong activation of shear layers, and the possible presence of hidden global modes described in Lin & Ogilvie, 2021), the stronger are the non-linear effects and induced zonal flows, resulting in larger departures from linear predictions, as we can see from Fig. 1. In the three non-linear simulations displayed at different forcing frequencies, we demonstrate that the final non-linear tidal dissipation rates are nicely explained by the injection of energy due to tidal power ($P_{\rm t} = \langle\rho\boldsymbol{u}_{\rm w}\cdot\boldsymbol{f}_{\rm t}\rangle$) predicted by separate linear simulations with initial background sheared flows (i.e. zonal flows are responsible for the departure from prior linear theory). Cylindrical sheared zonal flows have been extracted from non-linear simulations after a steady state has been reached, and these are then implemented in the momentum equation similar to Baruteau & Rieutord (2013)'s, except for the use of a tidal forcing and a more complex zonal flow profile here.

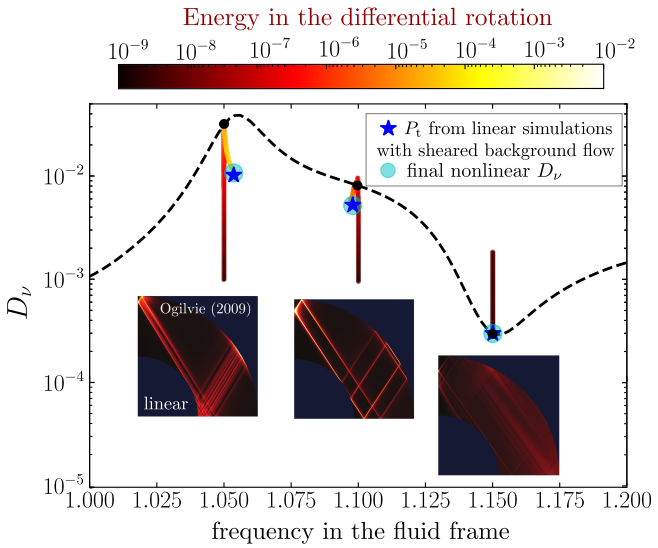

Figure 1: [Adapted from Astoul & Barker (2022)]. Tidal dissipation D_ν versus frequency in the rotating frame indicating energy in the zonal flows as it evolves during the simulations (colorbar). Linear dissipation predictions are indicated by dashed lines and black dots indicate three specific frequencies where non-linear simulations are launched. The tidal forcing amplitude is $C_{\rm T} \approx 9\cdot 10^{-3}$.

4.2 Waves and zonal flow interactions

For tidal forcing amplitudes of the order of $C_{\rm T} \lesssim 10^{-2}$ or lower, the departure from linear tidal dissipation predictions stays moderate to low (less than an order of magnitude of discrepancy for $E = 10^{-5}$), with the non-linear tidal dissipation often being reduced, which is explained well quantitatively by the emerging zonal flows and their back-reaction on the waves. For higher tidal forcing amplitudes, this is not always true, as evidenced in Fig. 2 for $C_{\rm T} = 5\cdot 10^{-2}$.

[3] These can be shown to be small in our problem (Astoul & Barker, 2022), but they can lead to unrealistic evolution of the total angular momentum in a spherical model, as observed in Favier *et al.* (2014) and demonstrated in Astoul & Barker (2022).

[4] https://magic-sph.github.io/

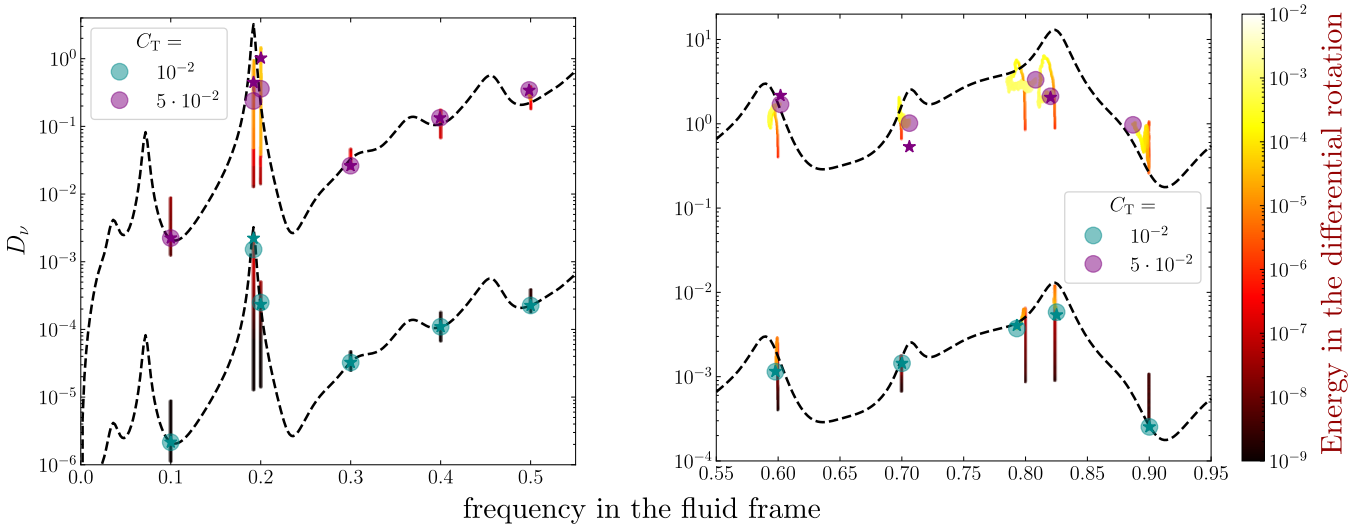

Figure 2: [Adapted from Astoul & Barker (2022)] Linear and non-linear tidal dissipation rates as in Fig. 1 as a function of tidal forcing frequency showing the energy inside the differential rotation, for two tidal forcing amplitudes (the upper curves and markers have been shifted by a factor of 10^3 for clarity). Stars indicate linear simulations with background zonal flows.

In several cases where the tidal power from linear simulations with background zonal flows does not balance the non-linear tidal dissipation rates, $P_t^{\rm linear} \neq D_\nu^{\rm nonlinear}$, we have discovered and characterised strong wave-wave and wave-zonal flow interactions leading to instabilities, that could be the cause of the mismatch. For $\omega = 0.2$, we evidenced parametric instabilities driven by triadic resonances that involved the coupling of the primary tidal waves (with azimuthal order $m = 2$) with daughter waves with different frequencies (and different azimuthal wavenumbers), as well as the excitation of superharmomics self-excited by the primary wave. The former wave-wave couplings lead to an "inertial wave energy cascade" also involving velocity components with odd azimuthal wavenumbers in the energy spectrum (e.g. in a box Jouve & Ogilvie, 2014; Le Reun *et al.*, 2017).

For cases with $\omega = 0.8$ or $\omega = 0.9$, a steady tidal power from linear simulations with respective background sheared flows at these frequencies is not obtained. In these simulations, the total kinetic energy grows exponentially possibly due to a shear instability. We demonstrated that the tidally forced inertial waves take energy from the mean flow and deposit it in a localised cylinder close to the poles that forms a corotation resonance. This only happens in the presence of differential rotation when the phase velocity of the wave matches the local zonal flow speed, which results in $\delta\Omega(s) = \omega/m$ (see e.g. for free inertial waves in a shell Baruteau & Rieutord, 2013; Astoul *et al.*, 2021, in a box). This phenomenon is visible in Fig. 3, where we observe that shear layers become curved close to the co-rotation resonance due to the strength of the shear there. These shear layers, whose widths are proportional to $E^{1/4}$, nicely follow curved attractors (in green) that become vertical when the waves approach the critical cylinder (dashed black lines). The attractors are drawn by solving the differential equation for the paths of characteristics of inviscid and free inertial waves:

$$\frac{{\rm d}z}{{\rm d}s} = \pm\sqrt{\frac{\kappa^2(s)}{\sigma^2(s)} - 1}, \tag{4}$$

with $\sigma = \omega - m\delta\Omega(s)$ the Doppler-shifted frequency ($= 0$ at the corotation resonance, which explains why the path is vertical there), and $\kappa = \sqrt{2\Omega_s(2\Omega_s + s\Omega_s')}$ is sometimes called the epicyclic frequency where $\Omega_s = \Omega + \delta\Omega(s)$ is the rotation rate in an inertial frame. A simple finite-difference method is used to compute the characteristics for a limited number of reflections between the inner and outer spheres, starting from the inner critical latitude θ (from the equator) satisfying:

$$\sin\theta = \frac{\sigma(\alpha R\sin\theta)}{\kappa(\alpha R\sin\theta)}. \tag{5}$$

Though a corotation resonance is also present in non-linear simulations for $\omega = 0.8$ and $\omega = 0.9$, it doesn't lead to the exponential growth of the kinetic energy as observed in these linear simulations with background zonal flows. A possible explanation is that the zonal flow adjusts continuously to the angular momentum deposition of inertial waves at the corotation resonance, while it is fixed in linear simulations. Nevertheless, this analysis indicates the potential importance of corotation resonances on the tidal response.

5 Conclusion and prospects

We have performed nonlinear hydrodynamical simulations of tidally-excited inertial waves in adiabatic and incompressible convective shells using a realistic body tidal forcing (Astoul & Barker, 2022). The wave/non-wavelike tidal flow decomposition allowed us to identify and remove unrealistic non-wavelike fluxes through the boundaries that cause unphysical evolution of the total angular momentum (discussed in detail in Astoul & Barker, 2022). Solving the new set

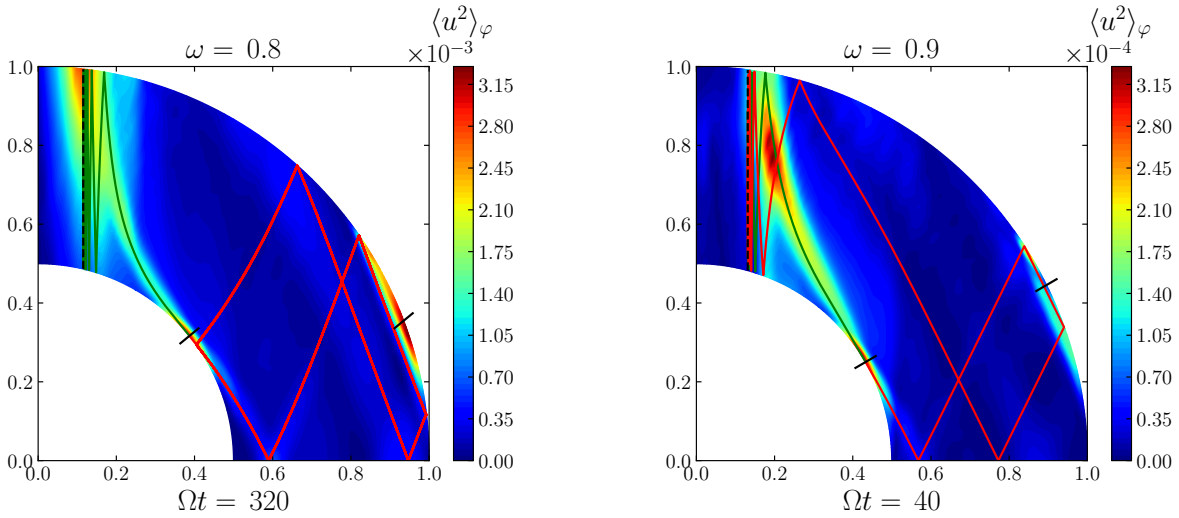

Figure 3: [Updated from Astoul & Barker (2022)] Azimuthally-averaged kinetic energy $\langle \boldsymbol{u}_{\rm w}^2 \rangle_\phi$ of tidally-excited inertial waves in one quadrant of the shell from linear simulations with a background zonal shear flow. The inertial wave characteristics are shown in green and red lines (colour indicating direction of propagation from the critical latitude), the co-rotation resonance in dashed lines and the critical latitude in black ticks. Interestingly, for $\omega = 0.8$ the 'lower' red path represents an attractor that forms a closed limit cycle.

of equations described in Eq. (3), which involves wavelike-wavelike nonlinearities only, we nevertheless observe the emergence of differential rotation in the form of zonal flows in the shell. When strong, they modify the tidal dissipation from prior linear predictions, and we find wave/wave and wave/zonal flow interactions to be important, leading to triadic and corotation resonances. When present, they may both further modify estimations of tidal dissipation rates from linear predictions with a sheared background flow. Parametric and possibly shear instabilities linked to these resonances are preferentially triggered for high tidal forcing amplitudes, low Ekman numbers (viscosities) or in thin convective shells (larger values of $\alpha < 1$). The computation of inertial wave characteristics with differential rotation sheds some light on the role of corotation resonances, but it remains to be understood why some linear simulations with background zonal flows featuring a corotation resonance exhibit instabilities while others do not. We are currently exploring the role of various shell thicknesses α representing the diversity of the internal structures of gaseous planets and their stellar hosts in order to quantify nonlinear tidal dissipation rates across a range of Hot Jupiter systems.

6 Acknowledgments

This research has been supported by STFC grants ST/R00059X/1, ST/S000275/1 and ST/W000873/1. A. Astoul acknowledges The Leverhulme Trust for their support with the award of an Early Career Fellowship.

7 *

References

Astoul, A. & Barker, A. J. 2022, MNRAS, 516, 2913.
Astoul, A., Park, J., Mathis, S., Baruteau, C., & Gallet, F. 2021, A&A, 647, A144.
Barker, A. J. 2020, MNRAS, 498, 2270.
Baruteau, C. & Rieutord, M. 2013, Journal of Fluid Mechanics, 719, 47.
Bekki, Y., Cameron, R. H., & Gizon, L. 2022, A&A, 666, A135.
Chernov, S. V., Ivanov, P. B., & Papaloizou, J. C. B. 2017, MNRAS, 470, 2054.
Favier, B., Barker, A. J., Baruteau, C., & Ogilvie, G. I. 2014, MNRAS, 439, 845.
Harre, J. V., Smith, A. M. S., Barros, S. C. C., Boué, G., Csizmadia, S., *et al.* 2023, A&A, 669, A124.
Jouve, L. & Ogilvie, G. I. 2014, Journal of Fluid Mechanics, 745, 223.
Le Reun, T., Favier, B., Barker, A. J., & Le Bars, M. 2017, Phys. Rev. Lett., 119, 034502.
Lin, Y. & Ogilvie, G. I. 2021, ApJL, 918, L21.
Maciejewski, G., Dimitrov, D., Fernández, M., Sota, A., Nowak, G., *et al.* 2016, A&A, 588, L6.
Maciejewski, G., Fernández, M., Sota, A., Amado, P. J., Dimitrov, D., *et al.* 2022, A&A, 667, A127.
Ogilvie, G. I. 2005, Journal of Fluid Mechanics, 543, 19.
Ogilvie, G. I. 2013, MNRAS, 429, 613.
Ogilvie, G. I. 2014, ARA&A, 52, 171.
Patra, K. C., Winn, J. N., Holman, M. J., Gillon, M., Burdanov, A., *et al.* 2020, AJ, 159, 150.
Tilgner, A. 2007, Phys. Rev. Lett., 99, 194501.
Vissapragada, S., Chontos, A., Greklek-McKeon, M., Knutson, H. A., Dai, F., *et al.* 2022, ApJL, 941, L31.
Weinberg, N. N., Sun, M., Arras, P., & Essick, R. 2017, ApJL, 849, L11.